PHYSICAL REVIEW LETTERS **134,** 196102 (2025)

High Pressure Synthesis of Rubidium Superhydrides

Mikhail A. Kuzovnikov,[1] Busheng Wang,[2] Xiaoyu Wang,[2] Tomas Marqueño,[1] Hannah A. Shuttleworth,[1]
Calum Strain,[1] Eugene Gregoryanz,[3,4,1] Eva Zurek,[2] Miriam Peña-Alvarez,[1] and Ross T. Howie[1,5,*]
[1]*Centre for Science at Extreme Conditions and School of Physics and Astronomy, University of Edinburgh,*
Edinburgh EH9 3JZ, United Kingdom
[2]*Department of Chemistry, State University of New York at Buffalo, Buffalo, 14260-3000, New York, USA*
[3]*SHARPS (Shanghai Advanced Research in Physical Sciences),*
68 Huatuo Rd, Bldg 3, Pudong, Shanghai, 201203, People's Republic of China
[4]*Key Laboratory of Materials Physics, Institute of Solid State Physics, Chinese Academy of Sciences (CAS),*
Hefei, Anhui 230031, People's Republic of China
[5]*Centre for High Pressure Science and Technology Advanced Research,*
1690 Cailun Rd, Bldg 6, Pudong, Shanghai, 201203, People's Republic of China

(Received 15 August 2024; accepted 12 March 2025; published 16 May 2025)

Through laser-heated diamond anvil cell experiments, we synthesize a series of rubidium superhydrides and explore their properties with synchrotron x-ray powder diffraction and Raman spectroscopy measurements, combined with density functional theory calculations. Upon heating rubidium monohydride embedded in H_2 at a pressure of 18 GPa, we form RbH_9-I, which is stable upon decompression down to 8.7 GPa, the lowest stability pressure of any known superhydride. At 22 GPa, another polymorph, RbH_9-II is synthesised at high temperature. Unique to the Rb-H system among binary metal hydrides is that further compression does not promote the formation of polyhydrides with higher hydrogen content. Instead, heating above 87 GPa yields RbH_5, which exhibits two polymorphs (RbH_5-I and RbH_5-II). All of the crystal structures comprise a complex network of quasimolecular H_2 units and H^- anions, with RbH_5 providing the first experimental evidence of linear H_3^- anions.

DOI: 10.1103/PhysRevLett.134.196102

Compression can profoundly change the electronic structure of materials, enabling the synthesis of novel compounds with unusual properties. In particular, high pressure has proven to be a very effective method to produce new materials with unusually high hydrogen content, or "superhydrides," some of which have exhibited high temperature superconductivity [1–4]. However, the vast majority of the known superhydrides require pressures above 100 GPa for their synthesis, with UH_7 having the lowest stability pressure of ~35 GPa [5,6].

The alkali metals have long been promising hosts to form superhydrides at comparatively lower pressures [7–11]. Despite the theoretical efforts in the prediction of these polyhydride structures, experimentally these compounds have seldom been explored and proved difficult to synthesize. Heating LiH at 130 GPa was claimed to induce a disproportionation into unidentified lithium polyhydrides containing H_2 units; however, in another study, no reaction between LiH and H_2 was observed up to pressures of 160 GPa at room temperature [12,13]. Two sodium polyhydrides, NaH_3 and NaH_7, were reported to form after laser heating NaH in a hydrogen medium at 40 GPa [14]. However, subsequent reports found NaH_3 to be the only stable phase between 14 and 80 GPa and attributed NaH_7 to be a misidentified CH_4-H_2 compound formed through sample contamination [15,16].

More promising candidates are the heavier alkali metal hydride systems, Rb-H and Cs-H, which are predicted to form compounds with high hydrogen content at pressures as low as 2 GPa, the lowest synthesis pressure of any binary metal superhydride [10,11,17]. Elemental rubidium reacts with hydrogen at ambient conditions to form RbH-I which adopts a face-centered cubic (fcc) crystal lattice [18]. Upon compression, RbH-I undergoes a phase transition to primitive simple cubic RbH-II above 2.2 GPa, before transforming to orthorhombic RbH-III at 85 GPa [18,19]. Experimentally, it remains unknown whether further reactions between any of the RbH phases and H_2 occur at high pressure.

Density functional theory (DFT) calculations predicted that RbH_9 with space group Pm should be stable at pressures between 2–20 GPa, while above this pressure, $P6_3/mmc$-RbH_9 should be stable up to 100 GPa [10]. At pressures above 20 GPa, RbH_5 with $Cmcm$ space group is

---

[*] Contact author: ross.howie@ed.ac.uk

predicted to be on the convex hull. While calculations indicated that the lowest point on the convex hull (structure with the most negative enthalpy of formation, ΔH_F) was RbH_9 at 10 GPa [10], by 20 GPa the magnitude of ΔH_F for the formation of *Cmcm*-RbH_5 was computed to be larger. This trend, where the hydrogen content in the lowest point on the convex hull decreased with increasing pressure, is unique to the alkali metal polyhydrides [8].

Interestingly, the crystal structure of the predicted *Cmcm*-RbH_5 comprises Rb^+ cations, quasimolecular H_2 units, and linear H_3^- anions. Although the triangular H_3^+ cations have been known since Thomson's early studies [20,21], the existence of H_3^- was only first reliably confirmed in discharge plasma experiments [22]. Thus from a chemical perspective, there is considerable interest in forming a crystalline lattice possessing H_3^- ions, which stabilize in a linear configuration. Despite the rich variety of predicted compounds and properties, together with routinely accessible synthesis conditions, the rubidium-hydrogen system has yet to be fully explored experimentally.

In this Letter, we report on the synthesis of rubidium superhydrides in a series of laser-heated diamond anvil cell experiments and study them through synchrotron x-ray diffraction and Raman spectroscopy measurements in combination with DFT calculations. Heating rubidium monohydride, RbH-II, in an H_2 medium at pressures of 18 GPa yields one polymorph of the RbH_9 superhydride, RbH_9-I, while heating at higher pressures of 22 GPa forms RbH_9-II, both of which have crystalline structures comprising quasimolecular H_2 units, Rb^+ cations, and H^- anions. Upon decompression, RbH_9-I is stable down to 8.7 GPa, the lowest pressure of stability of any superhydride found to date. Surprisingly, compression above 87 GPa and laser heating did not result in the formation of hydrides with higher hydrogen content. Instead, we observe the formation of an RbH_5 polymorph, RbH_5-II, which transforms to RbH_5-I upon decompression. Both RbH_5 phases exhibit the Raman signatures of linear H_3^- units. This is the first observation of H_3^- ions in a crystalline lattice.

Due to its reactivity in air, rubidium (99.75% purity, Alfa Aesar) was loaded into diamond anvil cells (DACs) in an inert argon atmosphere. The sample chamber was hermetically sealed and the DAC was transferred to a high-pressure gas loading apparatus, whereby hydrogen (99.9995% purity, BOC) was loaded at a pressure of 0.2 GPa. Hydrogen was always in excess, serving both as a reagent and the pressure-transmitting medium. Pressure was determined either through the equation of state of gold in x-ray diffraction measurements [23] or by Raman measurements through the intramolecular vibrational (vibron) frequency of excess H_2 [24]. A complete description of the experimental and computational methodology together can be found in the Supplemental Material (SM) [25].

After hydrogen was loaded into the sample chamber, the Rb metal precursor converted into transparent RbH on the timescale of a few minutes and, as expected, no Raman activity was observed for either RbH-I or RbH-II [18]. Upon compression at 297 K, the bulk RbH-II does not react further with excess H_2 up to at least 94 GPa, as evidenced by x-ray diffraction [the $V(P)$ data for RbH are shown by the red crosses in Fig. 2(a)]. In contrast to previous work, we did not observe a transformation from RbH-II to a RbH-III phase at 85 GPa. This could be attributed to a lack of hydrostaticity in previous data [18].

Laser heating RbH-II in an H_2 medium at pressures between 18 and 22 GPa to temperatures in excess of 1500 K produced a new hydride [Fig. 1(a)]. Rietveld refinement of its crystal structure indicates that the Rb atoms adopt a slightly distorted hexagonal close-packed (*hcp*) metal lattice with space group *Cmcm* and four atoms per unit cell (see Fig. 1(a) and Table SMII for lattice parameters [25]). The reaction is associated with a large volume increase of 32.9 Å^3/Rb atom at 19 GPa, and we estimate this hydride to have an RbH_9 composition using the volume of H_2 from Ref. [53]. As such, we henceforth

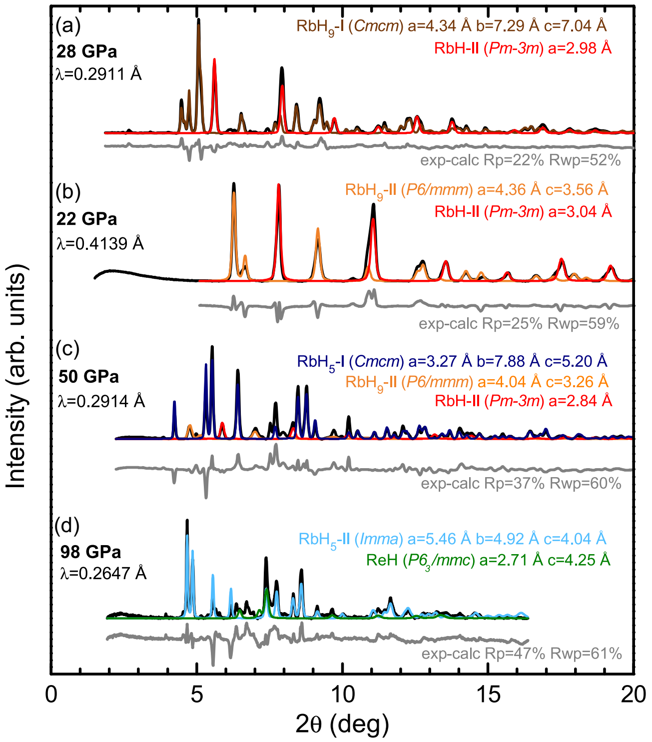

FIG. 1. Representative x-ray powder diffraction patterns and the results of the Rietveld refinements of (a) RbH_9-I at 28 GPa (brown), (b) RbH_9-II at 22 GPa (orange), (c) RbH_5-I at 50 GPa (dark blue), and (d) RbH_5-II at 98 GPa (light blue). The experimental data are shown by the black curves, and the refinement residuals are shown by the gray curves. The calculated contribution from RbH-II is shown in red, while ReH (from the gasket) is in green.

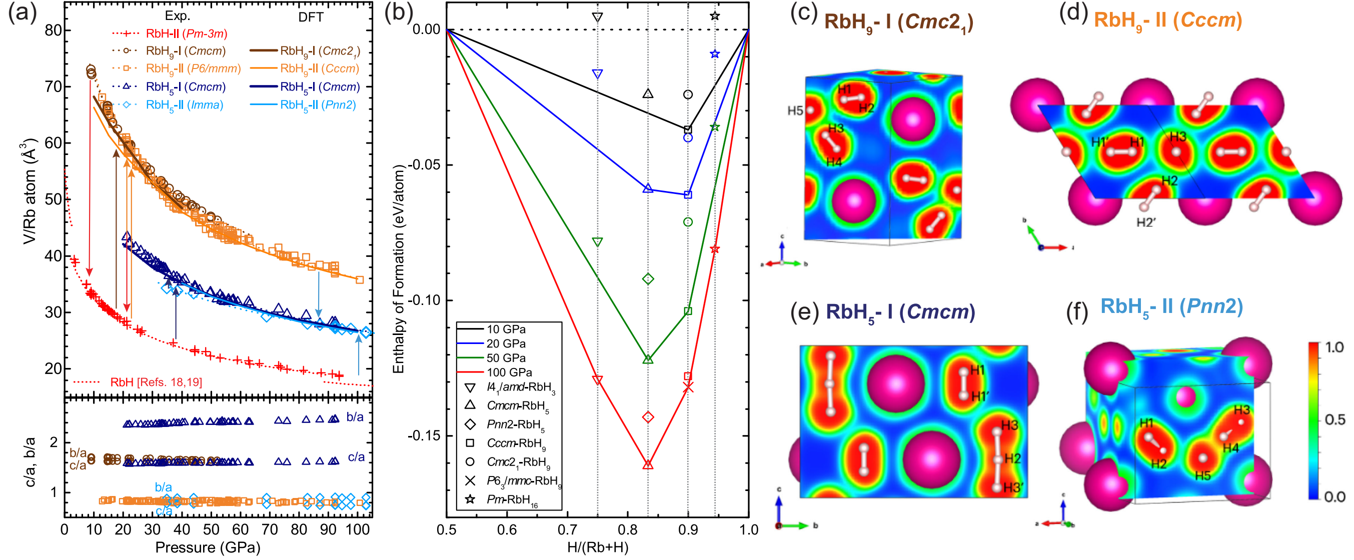

FIG. 2. (a) Volume as a function of pressure for the observed rubidium hydrides (top) and their b/a and c/a ratios (bottom). The dotted red curve shows the literature $V(P)$ data for RbH [18,19], dashed curves indicate the Birch-Murnaghan fits with parameters listed in Table SMIII in Supplemental Material [25], and solid curves show the DFT predictions. Vertical arrows show minimal pressures at which the phase transitions were observed upon compression after heating and maximal pressures at which they were observed upon decompression. (b) Formation enthalpies (ΔH_F) predicted by DFT for rubidium polyhydride phases (represented as different symbols) with respect to RbH + H_2 at 10 GPa (black), 20 GPa (blue), 50 GPa (green), and 100 GPa (red). Solid lines illustrate the convex hull. Calculated ELF plots for (c) $Cmc2_1$-RbH_9 at 20 GPa, (d) $Cccm$-RbH_9 at 50 GPa, (e) $Cmcm$-RbH_5 at 50 GPa, (f) $Pnn2$-RbH_5 at 50 GPa. $Cmcm$-RbH_5 possesses a linear symmetric H_3^- anion represented by atoms denoted H2, H3, and H3'. $Pnn2$-RbH_5 possesses an asymmetric H_3^- anion comprised of atoms denoted H3, H4, and H5.

refer to this phase as RbH_9-I. The $V(P)$ data, shown by the brown circles in Fig. 2(a), fit well with a Birch-Murnaghan equation of state, shown by the dashed brown line, suggesting that this phase has pressure-independent composition (see Table SMIII for equation of state parameters [25]). Decompression of RbH_9-I at room temperature results in the decomposition into RbH-II at 8.7 GPa. This is the lowest pressure of stability of any known superhydride. The absence of any decomposition products other than RbH and H_2 confirms that RbH_9-I is a binary rubidium hydride (see Fig. SM2 [25]).

Laser heating either RbH-II + H_2 or RbH_9-I + H_2 between 22 GPa and 56 GPa results in the formation of another polymorph, RbH_9-II. X-ray diffraction reveals that the Rb atoms are arranged in a primitive simple hexagonal lattice with the space group $P6/mmm$ [Fig. 1(b)]. This phase is marginally denser than RbH_9-I, and at 24 GPa its atomic volume is smaller by 0.8 Å^3/Rb atom, suggesting that their compositions are similar [see dashed orange curve in Fig. 2(a)]. Upon compression at room temperature, RbH_9-II persists up to at least 101 GPa, while upon decompression it transforms back to RbH_9-I at 14 GPa (Fig. SM2 [25]).

Due to negligible x-ray scattering by hydrogen atoms compared to the heavy Rb host, x-ray diffraction measurements cannot resolve the hydrogen positions in the crystal structure. As such, we have performed a constrained DFT-based crystal structure search for stable structures in the Rb-H system up to 100 GPa using the XTALOPT evolutionary algorithm [54,55] interfaced with VASP [56,57], and employing the GGA-PBE parametrization (see SM for details [25,58]). The calculated convex hulls of the Rb-H system at selected pressures are shown in Fig. 2(b). At pressures between 15 and 50 GPa, we find a structure with space group $Cccm$ [Fig. 2(d)], Table SMIV [25]) with a formation enthalpy that lies on the hull. This structure has a Rb sublattice very similar to that experimentally observed for RbH_9-II ($P6/mmm$), but with a small orthorhombic distortion. This distortion could be explained by our neglect of the quantum and anharmonic nature of the light hydrogen nuclei in our DFT calculations [59]. RbH_9-II and the theoretically predicted $Cccm$-RbH_9 have similar atomic volumes, as shown by the solid and dashed orange curves in Fig. 2(a), and c/a ratios in the hexagonal axes. Furthermore, our calculations find another RbH_9 polymorph with the space group $Cmc2_1$ and a Rb sublattice similar to that of RbH_9-I [Fig. 2(c), Table SMIV [25]). This $Cmc2_1$-RbH_9 structure is 15 meV/atom above $Cccm$-RbH_9 on the convex hull at 10 GPa at 0 K and within the clamped nuclei approximation [Fig. 2(b)]; however, both temperature and pressure can affect the relative stability (Fig. SM13 [25]). The atomic volumes of $Cmc2_1$-RbH_9 and the experimentally observed RbH_9-I ($Cmcm$) are comparable, as shown by the solid and dashed brown curves in Fig. 2(a). Thus, *Cccm*-RbH_9 and *Cmc*2_1-RbH_9 can serve as good approximants for the synthesized RbH_9-II and RbH_9-I phases, respectively.

Among all known binary hydride systems, higher pressure conditions generally facilitate further hydrogenation. Unique to the Rb-H system is that higher pressures do not promote the formation of even higher hydrogen content hydrides, but upon heating above 87 GPa, RbH_9-II partially decomposes into a new compound, which we denote as RbH_5-II. To the best of our knowledge, this represents the first experimental realization of pressure-induced decomposition in metal hydrides. Rietveld refinement of the RbH_5-II crystal structure [Fig. 1(d)] reveals a β-Sn-type metal lattice with an orthorhombic distortion, space group *Imma* [Fig. 1(d)]. RbH_5-II is stable upon compression to at least 103 GPa [Fig. 2(a)], while upon decompression below 35 GPa it undergoes a structural transition to another polymorph, RbH_5-I (Fig. SM4 [25]). The XRD pattern of RbH_5-I, shown in Fig. 1(c), is well described by the orthorhombic *Cmcm*-RbH_5 crystal structure, previously predicted in Ref. [10]. The crystal structure of RbH_5-I [Fig. 2(e)] is reminiscent of RbH_9-I; however, the atomic volume of RbH_5-I is much smaller and the distortion of the *hcp* lattice of metal atoms is much larger (Table SMII) [25]. Comparison of the atomic volumes demonstrates that RbH_5-I is marginally less dense than RbH_5-II across the studied pressure range [dark and light blue dashed curves in Fig. 2(a)]. We also found that RbH_5-I could be formed between 38 and 56 GPa if the amount of H_2 is insufficient to promote the formation of RbH_9-II. RbH_5-I persists upon room-temperature compression up to at least 92 GPa, while upon decompression it transforms to RbH_9-II and RbH-II below 21 GPa (Fig. SM5 [25]).

Our DFT calculations indicate that RbH_5-I lies on the convex hull between 20 and 100 GPa [Fig. 2(b)], while a computational search for structural candidates for RbH_5-II found a hypothetical compound with *Pnn*2 space group [Fig. 2(f), Table SMIV [25]). Although consistent with the x-ray diffraction data, this compound is about 20 meV/atom above *Cmcm*-RbH_5 on the convex hull at 100 GPa [red diamond and triangle in Fig. 2(b)]. Nevertheless, a reasonable agreement between the experimental [dashed light blue curve in Fig. 2(a)] and predicted (solid light blue curve) volumes of RbH_5-II verifies the assignment of its hydrogen content.

All of the synthesized rubidium superhydrides exhibit rich Raman activity [Fig. 3(a)], dominated by modes between 3700 and 4300 cm^{-1}, which are characteristic of hydrides hosting quasimolecular H_2 [60]. In addition there are complex spectra in the region below the diamond Raman line at 1330 cm^{-1}, which are attributed to librons of trapped quasimolecular H_2. At low pressures, the Raman spectra of both RbH_9 phases are dominated by two intense H-H stretching modes, which differ in frequency due to differing molecular environments. RbH_9-I exhibits an intense H-H stretching mode at ~3825 cm^{-1} at 20 GPa, which softens with pressure up to 30 GPa, after which it increases in frequency, and another mode at ~4070 cm^{-1}, which hardens with pressure [brown circles in Fig. 3(b)]. RbH_9-II also has two H-H stretching modes (3860 & 3920 cm^{-1} at 30 GPa), which harden and merge upon compression [orange squares in Fig. 3(b)]. The calculated Raman spectra of *Cmc*2_1-RbH_9 and *Cccm*-RbH_9 are in qualitative agreement with that observed experimentally for RbH_9-I and RbH_9-II (see Fig. SM12 [25]).

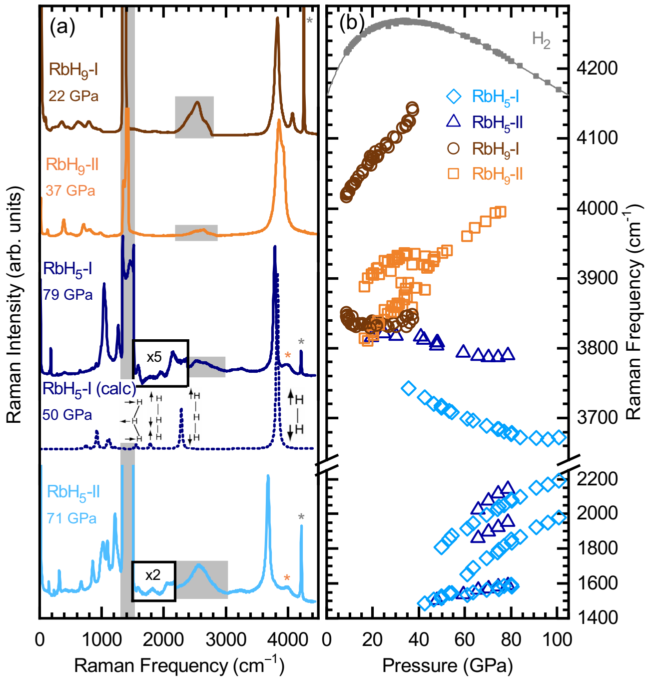

FIG. 3. (a) Representative Raman spectra of RbH_9-I (brown) at 22 GPa, RbH_9-II at 37 GPa (orange), RbH_5-I at 79 GPa (dark blue), and RbH_5-II at 71 GPa (light blue). The calculated Raman spectrum of *Cmcm*-RbH_5 at 50 GPa is shown as a dashed dark blue line, while the calculated Raman spectra of the other phases can be found in Fig. SM12 [25]. Raman excitations from the diamond anvils are highlighted by the gray shaded areas, gray asterisks indicate the vibron from the excess H_2 medium, and the orange asterisk indicates trace RbH_9-II. (b) Raman shift as a function of pressure of the vibrons attributed to quasimolecular hydrogen and H_3^- units within the rubidium lattices. The gray symbols correspond to the vibron frequency of the surrounding H_2 medium, while the gray line is the frequency of pure H_2 from prior studies [24]. The pressure dependence of the low frequency modes are given in Fig. SM3 [25].

In contrast to the RbH_9 phases, the H_2 vibron in the RbH_5 phases continuously softens with pressure [dark blue triangles and light blue diamonds in Fig. 3(b)]. Additionally, the Raman spectrum of RbH_5-I exhibits low intensity modes at 1590, 1960, and 2150 cm^{-1} [outlined with a black rectangle in Fig. 3(a)] that can be assigned to the bending, antisymmetric and symmetric stretching modes of linear H_3^- anions, respectively [10].

This signature is also observed for RbH_5-II, albeit at slightly different frequencies, indicative of differing molecular environments. This is the first experimental observation of H_3^- units in the solid state. It is interesting to note that in typical linear triatomic molecules, like CO_2, the antisymmetric stretching mode has a higher frequency than the symmetric one, in contrast to what is predicted for H_3^- in *Cmcm*-RbH_5. According to our calculations, the shortest H-H interatomic distance in the H_3^- anions, $r(\text{H-H}) \approx 0.95$ Å is larger than that in quasimolecular H_2 units, $r(\text{H-H}) \approx 0.79$ Å at 50 GPa in *Cmcm*-RbH_5. This explains the lower vibrational frequencies of H_3^- compared to those of the hosted H_2 units. We have calculated the electron localization function (ELF) and the integrated crystal orbital Hamilton population (-ICOHP) to explore the chemical bonding of the hydrogen motifs. In both RbH_9 phases there are H_2 units and isolated H^-, while both the calculated ELF and -ICOHP clearly shows the presence of H_2 and symmetric H_3^- units in *Cmcm*-RbH_5. In *Pnn*2-RbH_5 there are weaker bonded assymetric H_3^- units (see Fig. 2(f) and Table SMVI [25]). This H_3^- anion has one short bond (H3-H4, bond distance 0.867 A) and one long one (H4-H5, bond distance 1.128 A) at 50 GPa.

Both the alkali and alkaline earth hydrides have been predicted to possess symmetric H_3^- units; however, experimental studies did not observe spectroscopic signatures [9–11,61–64]. This may be because the H_3^- units are a result of transient molecularization between H_2 and H^- and the lifetime is shorter than the Raman effect, or because they are not stable [64]. In the case of RbH_5, the H_3^- are not only observable in the timescale of the experiment, but the linewidths of the Raman bands (which are indicative of lifetime) are on the order of the hosted H_2 mode, demonstrating that it is nontransient.

Recently, rubidium superhydride phases were claimed to form as the disproportionation products of $RbNH_2BH_3$; however, the interpretation of the results were heavily based on this present study [65,66]. The Rb-H phases reported were observed between 1.8 GPa and 8 GPa, below the stability field of any binary rubidium superhydride found here, and their crystal structures are inconsistent with our reported x-ray diffraction data [25]. Nevertheless, the rubidium-hydrogen system is the first to produce superhydride phases at pressures within the accessibility regime of large-volume high pressure chambers, such as the Toroid [67] and the Paris-Edinburgh press [68]. This presents an opportunity for neutron scattering studies to explore further the diverse hydrogen species within these fascinating materials.

Acknowledgments—The work was supported by the European Research Council (ERC) under the European Union's Horizon 2020 research and innovation program (Grant Agreement No. 948895, MetElOne) and a UKRI Future Leaders fellowship (Mrc-Mr/T043733/1). E. Z. acknowledges the U.S. National Science Foundation (DMR-2136038) for financial support and the Center for Computational Research at SUNY Buffalo for computational support (http://hdl.handle.net/10477/79221). Portions of this work were performed at GeoSoilEnviroCARS (The University of Chicago, Sector 13), Advanced Photon Source (APS), Argonne National Laboratory. GeoSoilEnviroCARS is supported by the National Science Foundation-Earth Sciences (EAR-1634415). This research used resources of the Advanced Photon Source, a U.S. Department of Energy (DOE) Office of Science User Facility operated for the DOE Office of Science by Argonne National Laboratory, under Contract No. DE-AC02-06CH11357. We would like to thank S. Chariton and V. B. Prakapenka for their assistance with the 13-ID beamline allocated under proposal GUP-81704. We acknowledge DESY (Hamburg, Germany), a member of the Helmholtz Association HGF, for the provision of beamline P02.2 at PETRA-III, allocated under proposal I-20220830, and we would like to thank Hanns-Peter Liermann and Timofey Fedotenko for their assistance. The ESRF (Grenoble, France) is acknowledged for providing access to beamlines ID27 and ID15B for beamtime HC-4878. We thank M. Mezouar, B. Wehinger, M. Hanfland, G. Garbarino and S. Gallego-Parra for beamline support. Part of the study was performed at I15, Diamond Light Source (Didcot, UK), under proposal CY30698-1; we would like to acknowledge C. Beavers for assistance in collecting the high-pressure data.

---

[1] M. Somayazulu, M. Ahart, A. K. Mishra, Z. M. Geballe, M. Baldini, Y. Meng, V. V. Struzhkin, and R. J. Hemley, Phys. Rev. Lett. **122**, 027001 (2019).

[2] A. Drozdov, P. Kong, V. Minkov, S. Besedin, M. Kuzovnikov, S. Mozaffari, L. Balicas, F. Balakirev, D. Graf, V. Prakapenka *et al.*, Nature (London) **569**, 528 (2019).

[3] P. Kong, V. S. Minkov, M. A. Kuzovnikov, A. P. Drozdov, S. P. Besedin, S. Mozaffari, L. Balicas, F. F. Balakirev, V. B. Prakapenka, S. Chariton, D. A. Knyazev, E. Greenberg, and M. I. Eremets, Nat. Commun. **12**, 5075 (2021).

[4] L. Ma, K. Wang, Y. Xie, X. Yang, Y. Wang, M. Zhou, H. Liu, X. Yu, Y. Zhao, H. Wang *et al.*, Phys. Rev. Lett. **128**, 167001 (2022).

[5] I. A. Kruglov, A. G. Kvashnin, A. F. Goncharov, A. R. Oganov, S. S. Lobanov, N. Holtgrewe, S. Jiang, V. B. Prakapenka, E. Greenberg, and A. V. Yanilkin, Sci. Adv. **4**, eaat9776 (2018).

[6] B. Guigue, A. Marizy, and P. Loubeyre, Phys. Rev. B **102**, 014107 (2020).

[7] P. Baettig and E. Zurek, Phys. Rev. Lett. **106**, 237002 (2011).

[8] E. Zurek, Comments Inorg. Chem. **37**, 78 (2017).

[9] J. Hooper and E. Zurek, J. Phys. Chem. C **116**, 13322 (2012).

[10] J. Hooper and E. Zurek, Chem. Eur. J. **18**, 5013 (2012).

[11] A. Shamp, J. Hooper, and E. Zurek, Inorg. Chem. **51**, 9333 (2012).

[12] C. Pépin, P. Loubeyre, F. Occelli, and P. Dumas, Proc. Natl. Acad. Sci. U.S.A. **112**, 7673 (2015).

[13] R. T. Howie, O. Narygina, C. L. Guillaume, S. Evans, and E. Gregoryanz, Phys. Rev. B **86**, 064108 (2012).

[14] V. V. Struzhkin, D. Y. Kim, E. Stavrou, T. Muramatsu, H.-k. Mao, C. J. Pickard, R. J. Needs, V. B. Prakapenka, and A. F. Goncharov, Nat. Commun. **7**, 1 (2016).

[15] T. Marqueno, M. A. Kuzovnikov, I. Osmond, P. Dalladay-Simpson, A. Hermann, R. T. Howie, and M. Pena-Alvarez, Front. Chem. **11**, 1306495 (2023).

[16] U. Ranieri, L. J. Conway, M.-E. Donnelly, H. Hu, M. Wang, P. Dalladay-Simpson, M. Peña-Alvarez, E. Gregoryanz, A. Hermann, and R. T. Howie, Phys. Rev. Lett. **128**, 215702 (2022).

[17] M. J. Hutcheon, A. M. Shipley, and R. J. Needs, Phys. Rev. B **101**, 144505 (2020).

[18] K. Ghandehari, H. Luo, A. L. Ruoff, S. S. Trail, and F. J. Disalvo, Mod. Phys. Lett. B **09**, 1133 (1995).

[19] H. D. Hochheimer *et al.*, Z. Phys. Chem. Neue Folge **143**, 139 (1985).

[20] J. J. Thomson O. M. F. R. S., London Edinburgh Dublin Phil. Mag. J. Sci. **24**, 209 (1912).

[21] C. A. Coulson, Math. Proc. Cambridge Philos. Soc. **31**, 244 (1935).

[22] W. Wang, A. K. Belyaev, Y. Xu, A. Zhu, C. Xiao, and X.-F. Yang, Chem. Phys. Lett. **377**, 512 (2003).

[23] S. M. Dorfman, V. B. Prakapenka, Y. Meng, and T. S. Duffy, J. Geophys. Res. **117**, B08210 (2012).

[24] R. T. Howie, C. L. Guillaume, T. Scheler, A. F. Goncharov, and E. Gregoryanz, Phys. Rev. Lett. **108**, 125501 (2012).

[25] See Supplemental Material at http://link.aps.org/supplemental/10.1103/PhysRevLett.134.196102 for a complete description of the experimental and computational methodology, which includes Refs. [27–53].

[26] H.-P. Liermann, Z. Konôpková, W. Morgenroth, K. Glazyrin, J. Bednarčik, E. E. McBride, S. Petitgirard, J. T. Delitz, M. Wendt, Y. Bican, A. Ehnes, I. Schwark, A. Rothkirch, M. Tischer, J. Heuer, H. Schulte-Schrepping, T. Kracht, and H. Franz, J. Synchrotron Radiat. **22**, 908 (2015).

[27] M. Merlini and M. Hanfland, High Press. Res. **33**, 511 (2013).

[28] V. Prakapenka, A. Kubo, A. Kuznetsov, A. Laskin, O. Shkurikhin, P. Dera, M. Rivers, and S. Sutton, High Press. Res. **28**, 225 (2008).

[29] S. Anzellini, A. K. Kleppe, D. Daisenberger, M. T. Wharmby, R. Giampaoli, S. Boccato, M. A. Baron, F. Miozzi, D. S. Keeble, A. Ross, S. Gurney, J. Thompson, G. Knap, M. Booth, L. Hudson, D. Hawkins, M. J. Walter, and H. Wilhelm, J. Synchrotron Radiat. **25**, 1860 (2018).

[30] C. Prescher and V. B. Prakapenka, High Press. Res. **35**, 223 (2015).

[31] W. Kraus and G. Nolze, J. Appl. Crystallogr. **29**, 301 (1996).

[32] Y. Akahama and H. Kawamura, J. Appl. Phys. **100**, 043516 (2006).

[33] H. K. Mao, J. Xu, and P. M. Bell, J. Geophys. Res. **91**, 4673 (1986).

[34] F. Birch, Phys. Rev. **71**, 809 (1947).

[35] M. Peña-Alvarez *et al.*, J. Phys. Chem. Lett. **11**, 6626 (2020).

[36] Y. Fukai, *The Metal-Hydrogen System*, 2nd ed. (Springer-Verlag, Berlin-Heidelberg, 2005), pp. 104–113.

[37] C. V. Storm, J. D. McHardy, S. E. Finnegan, E. J. Pace, M. G. Stevenson, M. J. Duff, S. G. MacLeod, and M. I. McMahon, Phys. Rev. B **103**, 224103 (2021).

[38] V. E. Antonov, A. I. Latynin, and M. Tkacz, J. Phys. Condens. Matter **16**, 8387 (2004).

[39] P. Avery, C. Toher, S. Curtarolo, and E. Zurek, Comput. Phys. Commun. **237**, 274 (2019).

[40] P. Avery and E. Zurek, Comput. Phys. Commun. **213**, 208 (2017).

[41] D. C. Lonie and E. Zurek, Comput. Phys. Commun. **183**, 690 (2012).

[42] B. Wang, K. P. Hilleke, S. Hajinazar, G. Frapper, and E. Zurek, J. Chem. Theory Comput. **19**, 7960 (2023).

[43] S. P. Ong *et al.*, Comput. Mater. Sci. **68**, 314 (2013).

[44] A. Savin, R. Nesper, S. Wengert, and T. F. Fässler, Angew. Chem., Int. Ed. Engl. **36**, 1808 (1997).

[45] P. E. Blöchl, Phys. Rev. B **50**, 17953 (1994).

[46] G. Kresse and D. Joubert, Phys. Rev. B **59**, 1758 (1999).

[47] H. Monkhorst and J. D. Pack, Phys. Rev. B **13**, 5188 (1976).

[48] S. Maintz, V. L. Deringer, A. L. Tchougréeff, and R. Dronskowski, J. Comput. Chem. **37**, 1030 (2016).

[49] R. S. Mulliken, J. Chem. Phys. **23**, 1833 (1955).

[50] C. Ertural, S. Steinberg, and R. Dronskowski, RSC Adv. **9**, 29821 (2019).

[51] C. J. Pickard and R. J. Needs, Nat. Phys. **3**, 473 (2007).

[52] L. Monacelli, I. Errea, M. Calandra, and F. Mauri, Nat. Phys. **17**, 63 (2021).

[53] J.-M. Joubert, Int. J. Hydrogen Energy **35**, 2104 (2010).

[54] D. C. Lonie and E. Zurek, Comput. Phys. Commun. **182**, 372 (2011).

[55] Z. Falls, P. Avery, X. Wang, K. P. Hilleke, and E. Zurek, J. Phys. Chem. C **125**, 1601 (2021).

[56] G. Kresse and J. Furthmuller, Phys. Rev. B **54**, 11169 (1996).

[57] G. Kresse *et al.*, Comput. Mater. Sci. **6**, 15 (1996).

[58] J. P. Perdew, K. Burke, and M. Ernzerhof, Phys. Rev. Lett. **77**, 3865 (1996).

[59] I. Errea, F. Belli, L. Monacelli, A. Sanna, T. Koretsune, T. Tadano, R. Bianco, M. Calandra, R. Arita, F. Mauri *et al.*, Nature (London) **578**, 66 (2020).

[60] M. Peña-Alvarez, J. Binns, M. Marqués, M. A. Kuzovnikov, P. Dalladay-Simpson, C. J. Pickard, G. J. Ackland, E. Gregoryanz, and R. T. Howie, J. Phys. Chem. Lett. **13**, 8447 (2022).

[61] J. Hooper, B. Altintas, A. Shamp, and E. Zurek, J. Phys. Chem. C **117**, 2982 (2013).

[62] Y. Chen, H. Y. Geng, X. Yan, Y. Sun, Q. Wu, and X. Chen, Inorg. Chem. **56**, 3867 (2017).

[63] W. Chen, D. V. Semenok, A. G. Kvashnin, X. Huang, I. A. Kruglov, M. Galasso, H. Song, D. Duan, A. F. Goncharov, V. B. Prakapenka *et al.*, Nat. Commun. **12**, 273 (2021).

[64] M. Marqués, M. Peña-Alvarez, M. Martínez-Canales, and G. J. Ackland, J. Phys. Chem. C **127**, 15523 (2023).

[65] D. Zhou, D. Semenok, M. Galasso, F. G. Alabarse, D. Sannikov, I. A. Troyan, Y. Nakamoto, K. Shimizu, and A. R. Oganov, Adv. Energy Mater. **14**, 2400077 (2024).

[66] M. Kuzovnikov, Synthesis of novel rubidium superhydrides under high-pressure, in *28th AIRAPT and 60th EHPRG International Conference* (2023), https://airdrive.eventsair.com/eventsairwesteuprod/production-iop-public/6f1b25d61ee04e1090f5e71352cb88c0.

[67] L. G. Khvostancev *et al.*, High Press. Res. **24**, 371 (2004).

[68] J. M. Besson, R. J. Nelmes, G. Hamel, J. S. Loveday, G. Weill, and S. Hull, Physica (Amsterdam) **180B**, 907 (1992).